PHYSICAL REVIEW B **96**, 024509 (2017)

Effect of disorder on superconductivity and Rashba spin-orbit coupling in $LaAlO_3$ /$SrTiO_3$ interfaces

G. Singh,[1,2] A. Jouan,[1,2] S. Hurand,[1,2] C. Feuillet-Palma,[1,2] P. Kumar,[3] A. Dogra,[3]
R. Budhani,[3,4] J. Lesueur,[1,2] and N. Bergeal[1,2]

[1]*Laboratoire de Physique et d'Etude des Matériaux, ESPCI Paris, PSL Research University, CNRS, 10 Rue Vauquelin, 75005 Paris, France*
[2]*Université Pierre and Marie Curie, Sorbonne-Universités, 75005 Paris, France*
[3]*National Physical Laboratory, Council of Scientific and Industrial Research (CSIR), Dr. K.S. Krishnan Marg, New Delhi-110012, India*
[4]*Condensed Matter Low Dimensional Systems Laboratory, Department of Physics, Indian Institute of Technology, Kanpur 208016, India*

(Received 5 October 2016; revised manuscript received 22 March 2017; published 18 July 2017)

A rather unique feature of the two-dimensional electron gas formed at the interface between the two insulators $LaAlO_3$ and $SrTiO_3$ is to host both gate-tunable superconductivity and strong spin-orbit coupling. In the present work, we use the disorder generated by Cr substitution of Al atoms in $LaAlO_3$ as a tool to explore the nature of superconductivity and spin-orbit coupling in these interfaces. We analyze the transport properties of three different samples whose only relevant difference is their elastic scattering time τ_e. A reduction of the superconducting T_c is observed with Cr doping consistent with an increase of electron-electron interaction in the presence of disorder. In addition, the evolution of spin-orbit coupling with gate voltage and Cr doping evidences a Dyakonov-Perel mechanism of spin relaxation ($\tau_{SO} \propto \tau_e^{-1}$) in the presence of a Rashba-type spin-orbit interaction.

DOI: 10.1103/PhysRevB.96.024509

Oxide interfaces involving band or Mott insulators such as $LaAlO_3/SrTiO_3$ and $LaTiO_3/SrTiO_3$ have attracted much attention in recent years due to the formation of a two-dimensional electron gas (2DEG) [1] whose quantum properties include, in particular, superconductivity [2,3], strong spin-orbit coupling (SOC) [4,5], and magnetism [6,7]. The interplay between these different properties makes $SrTiO_3$-based interfaces particularly interesting from fundamental as well as technological perspectives [8–11]. The conducting interface is identified as two-dimensional in nature, with a typical thickness ∼10 nm, smaller than the Fermi wavelength in the normal state, and smaller than the superconducting coherence length [3,12–14]. Electrons are confined within a quantum well which accommodates different bands built on the anisotropic t_{2g} orbitals of the Ti ions [15]. A key feature of these interfacial 2DEGs lies in the possibility to continuously tune the electron density by electric field effect [16]. As a result, gate-tunable superconductivity was achieved both in back-gate [17,18] and top-gate geometry [19,20]. For strong carrier depletion, a superconductor-to-insulator quantum phase transition was observed [18,19].

Transport measurements indicate that the nature of the SOC is most likely of the Rashba type as expected in an asymmetric quantum well [4,5,19]. The SOC strength reaches values of several meV, which is significantly larger than the ones found in semiconducting heterostructures. In addition, its intensity can be modulated with a gate voltage.

Because of 2D confinement, it is expected that the electronics properties of these interfaces should be strongly affected by external dopants, hence providing a way to explore their fundamental nature. Fix *et al.* reported a quenching of electron density and mobility in $LaAlO_3/SrTi_{1-x}R_xO_3$ when doped by Mn [21–23], while Sanders *et al.* recently observed that 2% doping of rare-earth ions Tm and Lu at the La site of $LaAlO_3$ does not significantly affect the electronic transport [24]. An increase of SOC in δ-doped $LaTiO_3/LaCrO_3/SrTiO_3$ interfaces was reported by Das *et al.* [25]. However, in these reports, it appears difficult to disentangle the respective roles of doping, disorder, and carrier density changes on the transport properties of the 2DEG.

In this article, we present a detailed analysis of the gate dependence of superconductivity and SOC in $LaAlO_3/SrTiO_3$ interfaces by controlled site substitution of Al by Cr. $LaCrO_3$ is an antiferromagnetic band insulator with a Neel temperature of 290 K and the $LaCrO_3/SrTiO_3$ heterostructure is insulating. However, the $LaAl_{1-x}Cr_xO_3/SrTiO_3$ interface was found to be conducting for the doping level used in this study [26,27]. We first show that Cr doping increases elastic scattering, that is the atomic scale disorder, without changing the carrier density. As a consequence, the differences in electronic transport properties between the three samples are solely determined by the elastic scattering time. Superconductivity is weakened by Cr doping, and disappears according to Finkelstein's theory [28] for which disorder is the only relevant parameter. On the other hand and independently, we showed through magnetoconductance that spin relaxation occurs by mean of a Dyakonov-Perel mechanism [29], and that the spin diffusion length is independent of the disorder as expected in that case.

For this study, three 10-u.c.-thick $LaAl_{1-x}Cr_xO_3$ films with doping $x = 0$, 0.1, and 0.2 were grown on TiO_2 terminated (001) $SrTiO_3$ substrate. The thin films were deposited at a constant substrate temperature of 750 °C in an oxygen pressure of 10^{-4} mbar. During the deposition, the layer-by-layer growth was monitored by reflection high-energy electron diffraction (RHEED). Further details about the growth and structural characterization can be found in Ref. [30]. A metallic gate is deposited on the backside of each $SrTiO_3$ substrate, and standard four-probe transport measurements were performed in a dilution refrigerator with a base temperature of 15 mK, equipped with a 6 T magnet.

Normal-state resistance and carrier density. We first investigate the effect of Cr doping on the sheet resistance and carrier density of the $LaAl_{1-x}Cr_xO_3/SrTiO_3$ interfaces. After cooling the sample to 3 K, the back-gate voltage was first swept to its maximum value of +200 V, while keeping the 2DEG at the electrical ground to ensure that no hysteresis will take

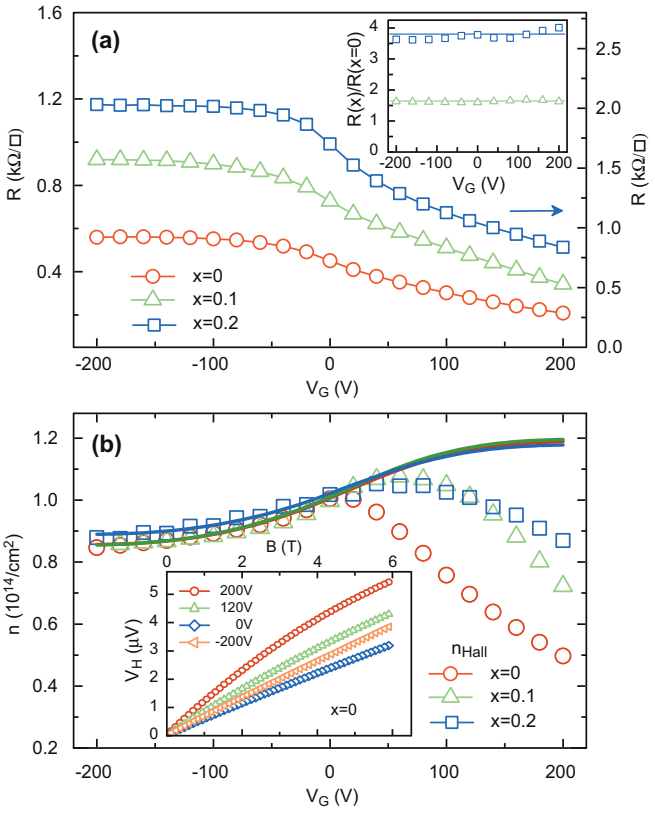

FIG. 1. (a) Sheet resistance R measured at $T = 3$ K as a function of gate voltage V_G for three $LaAl_{1-x}Cr_xO_3/SrTiO_3$ samples corresponding to doping $x = 0$ (left axis), $x = 0.1$ (left axis), and $x = 0.2$ (right axis). Inset: Sheet resistance of the $x = 0.1$ and $x = 0.2$ samples normalized by the sheet resistance of the $x = 0$ sample. Straight lines are guides for the eyes. (b) Carrier density extracted at $T = 3$ K from low-magnetic-field Hall effect measurements (n_H, open symbols) and from capacitance measurements (n, full lines, same color code) [34]. Inset: Hall voltages V_H as a function of the magnetic field B of the $x = 0$ sample measured for different V_G.

place upon further gating [31]. As expected when depleting the quantum well, the sheet resistance R of the three samples continuously rises when the gate voltage is decreased down to -200 V [Fig. 1(a)]. The absolute value of the sheet resistance for a given gate voltage V_G increases with x, indicating either an enhancement of scattering or a reduction of the carrier density with Cr doping.

To determine the carrier density in the 2DEG, we performed Hall effect measurements as a function of V_G for the different samples. As already reported in the literature [17,32,33], the Hall voltage is linear with magnetic field in the low-doping regime ($V_G < 0$) [inset of Fig. 1(b)] and the carrier density is correctly extracted from the slope of the Hall voltage V_H (i.e., $n_H = IB/eV_H$, where I is the bias current and B is the magnetic field). This is no longer the case in the high-doping regime ($V_G > 0$), where V_H is not linear with B, which is a sign of a multiband transport (see Supplemental Material [34]). In this case, n_H measured in the $B \to 0$ limit [see symbols in Fig. 1(b)] is not the carrier density. This explains why n_H surprisingly decreases at high gate voltage, while more electrons are added in the quantum well. The true variation of the carrier density n can be retrieved by measuring the capacitance C between the 2DEG and the gate [17]. The added charges upon gating is given by the integral of C over the gate voltage range [solid lines in Fig. 1(b)] (see Supplemental Material [34]). The absolute value n is calculated by assuming that for negative voltages, $n = n_H$ (one band transport), which is well verified experimentally [Fig. 1(b)]. Note that $n \sim 1\times 10^{14}\ e^-\ \mathrm{cm}^{-2}$ for $V_G = 0$, a value not too far from the number predicted by the polarization catastrophe scenario ($\simeq 3.3 \times 10^{14}\ e^-\ \mathrm{cm}^{-2}$) [35].

Remarkably, as evidenced in Fig. 1(b), the sheet carrier density n does not depend on Cr doping within the error margins in this doping range (higher Cr doping leads to a significant reduction of carrier density [30]). The increase of sheet resistance R with x is therefore only due to a reduction of the elastic scattering time τ_e. Within a simple Drude model, one expects $R(x)/R(x = 0) = \tau_e(x = 0)/\tau_e(x)$ to be constant, independent of the gate voltage. This is well verified in the inset of Fig. 1(a), where $R(x)/R(x = 0)$ is plotted for $x = 0.1$ and $x = 0.2$. Very small deviations occur for the highest value of V_G likely due to multiband transport. The first conclusion of this study is that Cr doping increases the atomic disorder in the system, and, at first order, only modifies the elastic scattering time τ_e. Even if the dopants are buried in the $LaAlO_3$ layer, they induce a slight perturbation of the potential seen by electrons, whose scattering time is therefore enhanced. Unlike changing the gate voltage that modifies several parameters at the same time, the Cr doping offers the possibility to study the influence of τ_e on superconductivity and SOC while keeping other parameters unchanged. In particular, this implies that for a given gate voltage, the quantum confinement is essentially identical for the three samples.

Superconductivity. The $x = 0$ sample displays a gate-tunable superconducting transition [Fig. 2(a)] as usually observed in $SrTiO_3$-based interfaces. A superconducting phase diagram can be drawn by plotting the transition temperature T_c (midpoint) extracted from $R(T)$ curves, as a function of V_G. It exhibits a partial dome shape with a maximum T_c of approximately 170 mK at an optimal electrostatic doping of $V_G \simeq 80$ V [Fig. 2(c)]. For the heavily doped sample ($x = 0.2$), no sign of superconductivity can be seen down to 20 mK (not shown). At intermediate doping ($x = 0.1$), the sample shows broad resistive transitions always saturating to a residual resistance at low temperature [Fig. 2(b)]. Despite signs of a superconducting condensation (such as the typical lowering of R below T_c), superconductivity is too weak to establish phase coherence across the whole sample. Nevertheless, a phase diagram similar to the one of the $x = 0$ sample is obtained, with a reduced midpoint T_c [Fig. 2(c)]. In the strongly underdoped regime (i.e., for gate values much lower than the one maximizing T_c), incomplete resistive transitions in $SrTiO_3$-based interfaces are systematically reported in the literature.

To analyze this behavior, Caprara *et al.* suggested that the $LaAlO_3/SrTiO_3$ interfaces should be described as an array of superconducting islands with a distribution of T_c coupled through a metallic 2DEG by the proximity effect [36,37]. An intrinsic mechanism of phase separation based on the nonrigidity of the bands in the interfacial quantum well has been proposed as a possible explanation for the formation of

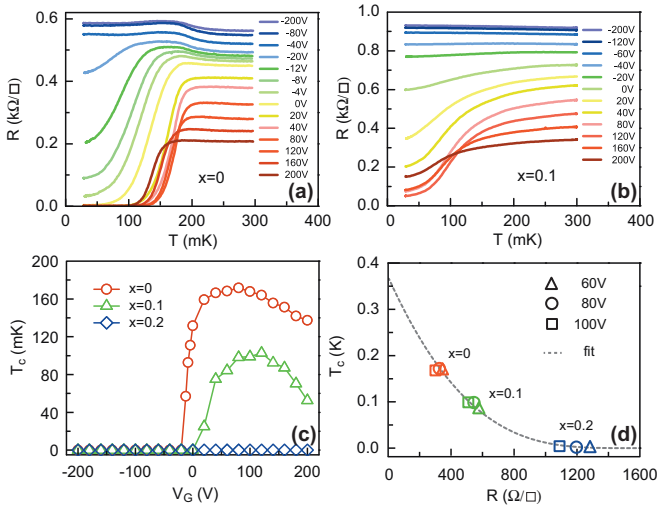

FIG. 2. (a) Sheet resistance R vs temperature T of the $x = 0$ sample for different V_G. (b) Same for the $x = 0.1$ $LaAl_{1-x}Cr_xO_3/SrTiO_3$ sample. (c) Superconducting T_c (defined as a 50% drop of R) as a function of V_G for the three samples. (d) T_c as a function of the sheet resistance measured at $T = 300$ mK, for the three samples and for three different V_G corresponding to the optimal electrostatic doping (i.e., the top of the T_c dome). Data are fitted by the Finkelstein's theory (see Supplemental Material [34]) (dotted line).

the islands [38]. At sufficiently low electrostatic doping, the superconducting fraction of the system becomes too low to enable a percolative superconducting transition, and, despite a sizable drop in resistance, a true zero resistive state is never reached at any arbitrary low temperature. Such scenario is illustrated by the $R(T)$ curves measured on the $x = 0$ sample at negative gate voltages [Fig. 2(a)].

The disorder induced by Cr-doping x, i.e., the decrease of the elastic scattering time τ_e, will affect both the superconducting islands and the metallic 2DEG. On the one hand, it lowers the Josephson coupling between islands: in the diffusive proximity effect, the normal coherence length reads $\xi_n = \sqrt{\frac{\hbar D}{k_B T}}$ where the electronic diffusion constant D is proportional to τ_e. This reduced coupling explains why the resistive transitions are broader in Cr-doped samples, and why the $R = 0$ state is never reached. On the other hand, it weakens superconductivity inside the islands, which is essentially measured by the midpoint T_c. According to Finkelstein's theory [28], disorder makes the screening of electron-electron interactions less efficient. As a consequence, the superconducting T_c is reduced and follows a universal law that depends on the sheet resistance inversely proportional to τ_e (see Supplemental Material [34]). To perform such analysis, we consider the T_c around the optimal electrostatic doping as in this region a BCS-like robust superconductivity has been evidenced [39]. A good agreement is obtained between experimental data and Finkelstein's theory, with a $T_c \simeq 350$ mK in the limit of null disorder, close to the one of doped bulk $SrTiO_3$ [Fig. 2(d)]. It indicates that the disorder strongly affects superconductivity in $LaAlO_3/SrTiO_3$ interfaces. This is valid both for as-grown disorder ($x = 0$) and the built-in one ($x = 0.1$ and $x = 0.2$) and can contribute to explain the spread in T_c observed in the literature.

Magnetotransport and spin-orbit coupling. The confinement of electrons at the $LaAlO_3/SrTiO_3$ interface generates a strong local electric field E_z perpendicular to the motion of the electrons, which gives rise to a Rashba-type spin-orbit coupling. It is described by the Hamiltonian $H_R = \alpha(k_y\sigma_x - k_x\sigma_y) = \vec{B}_R(\vec{k}) \cdot \vec{\sigma}$, where α is the coupling constant, $\vec{\sigma}$ are the Pauli matrices, and $\vec{B}_R(\vec{k})$ is the Rashba magnetic field whose direction and amplitude depend on the electron momentum $\vec{k}$ [40,41]. The spin of an electron propagating in the E_z electric field precesses around $\vec{B}_R(\vec{k})$ between two scattering events which causes a continuous spin dephasing, a mechanism known as the Dyakonov-Perel relaxation process [29]. The randomization of the precession direction by collisions results in a corresponding spin relaxation time that varies inversely with the elastic scattering time ($\tau_{SO} \propto \tau_e^{-1}$). This is different from the Elliot-Yafet mechanism where the collisions of an electron with an impurity can generate a direct spin flip which is characterized by a relaxation time proportional to the elastic scattering time ($\tau_{SO} \propto \tau_e$).

In a 2D system, τ_{SO} can be evaluated by analyzing how this additional spin relaxation mechanism modifies the weak localization corrections to the magnetoconductance $\Delta\sigma(B) = \sigma(B) - \sigma(0)$ [42,43]. In the following, we study the effect of Cr doping on SOC by measuring the conductance of the 2DEG as a function of a magnetic field applied perpendicular to the sample plane. The curves were fitted with the Maekawa-Fukuyama formula [19,42] in the diffusive regime, neglecting the Zeeman splitting,

$$\frac{\Delta\sigma(B)}{G_0} = -\psi\left[\frac{1}{2} + \frac{Be}{B}\right] + \frac{3}{2}\psi\left[\frac{1}{2} + \frac{B_\phi + B_{SO}}{B}\right] - \frac{1}{2}\psi\left[\frac{1}{2} - \frac{B_\phi}{B}\right] - \left[\frac{B_\phi + B_{SO}}{Be}\right] - \frac{1}{2}\ln\left[\frac{B_\phi + B_{SO}}{B_\phi}\right] - A_K\frac{\sigma(0)}{G_0}B^2. \quad (1)$$

Here, ψ is the digamma function, $G_0 = \frac{e^2}{\pi h}$ is the quantum of conductance, and B_e, B_ϕ, and B_{SO} are the elastic, inelastic, and spin-orbit effective fields, respectively. They are related to the elastic scattering time τ_e, the inelastic scattering time τ_Φ, and the spin-orbit relaxation time τ_{SO} by the expressions $B_e = \hbar/(4eD\tau_e)$, $B_\Phi = \hbar/(4eD\tau_\Phi)$, and $B_{SO} = \hbar/(4eD\tau_{SO})$, where $D = \frac{1}{2}v_F^2\tau_e$ is the electronic diffusion constant in two dimensions (v_F is the Fermi velocity). A_K is the Kohler term that accounts for orbital magnetoconductance. We did not need to include additional spin-flip scattering time in the analysis to fit our data, whatever the Cr-doping level. This indicates that electrons in the 2DEG do not interact with localized spins in this low Cr-doping regime. Figure 3(a) displays the magnetoconductance of the $x = 0.2$ sample measured at $T = 3$ K, for V_G ranging between ± 200 V, and fitted by Eq. (1). A very good agreement is obtained between the experimental data and the theory over the whole electrostatic gating range for this sample as well as for the other ones (see Supplemental Material [34]).

For large negative V_G, a positive magnetoconductance is observed consistently with weak localization in the presence of a weak SOC. When V_G is increased, the magnetoconductance becomes negative because of enhanced SOC. Beyond

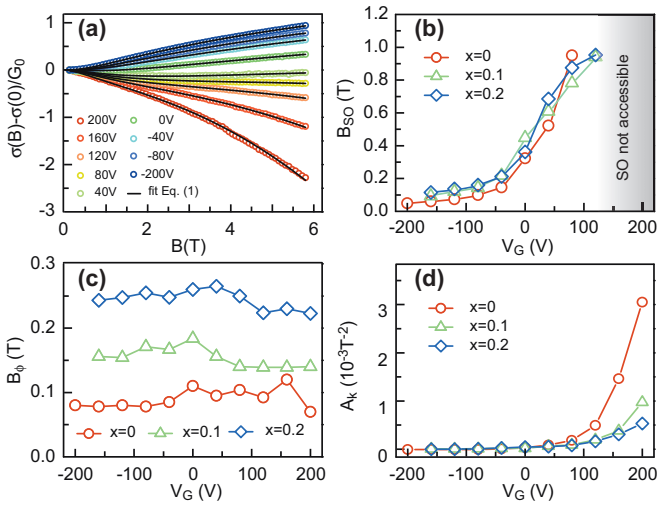

FIG. 3. (a) Normalized magnetoconductance as a function of out-of-plane magnetic field B of the $x = 0.2$ sample for different V_G (open symbols) fitted with Eq. (1). (b)–(d) Fitting parameters B_{SO}, B_ϕ, and A_K as a function of V_G for the three samples ($x = 0$, 0.1, 0.2). In the gray zone in (b), B_{SO} and B_ϕ are determined with reduced accuracy (see text).

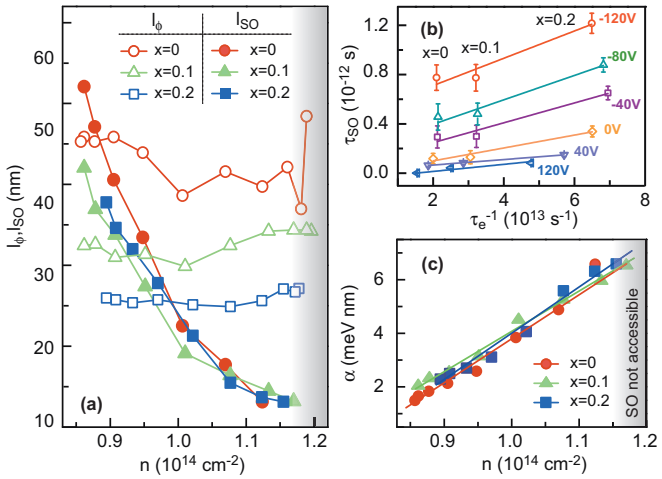

FIG. 4. (a) Spin-orbit precession length ℓ_{SO} (filled symbols) and phase coherence length ℓ_ϕ (open symbols) as a function of the total carrier density n. Beyond carrier density 1.16×10^{14} e^- cm^{-2}, the estimated values of ℓ_{SO} are not reliable since scattering is dominated by orbital magnetoconductance. (b) Spin-orbit relaxation time τ_{SO} as a function of τ_e^{-1} for selected V_G showing a linear relation in agreement with a Dyakonov-Perel relaxation mechanism. (c) Spin-orbit coupling constant α (filled symbols) as a function of n for the three samples. Solid lines are linear fits of the data. In the gray zones in (a) and (b), ℓ_{SO}, ℓ_ϕ, and α are determined with reduced accuracy (see text).

$V_G \sim 150$ V, the mobility of the 2DEG increases, and so does the A_K coefficient [see Fig. 3(d)], which is proportional to the square of it [44]. In that situation, Kohler's contribution dominates over the weak localization correction, and the determination of B_ϕ and B_{SO} becomes less accurate.

Figure 3(c) shows the inelastic field B_ϕ as a function of gate voltage for different Cr doping, $x = 0$, 0.1, and 0.2. B_ϕ does not show any significant dependence on V_G for the three samples, but increases clearly with doping x. This is a direct consequence of the reduction of the elastic scattering time τ_e that appears in the expression of B_ϕ [$B_\phi \propto (\tau_e \tau_\Phi)^{-1}$]. The inelastic scattering time τ_Φ is independent of x since it is dominated by electron-electron interactions [3,19] and the variation of B_ϕ with x is determined by the variation of τ_e. This is rather well verified within the experimental margin errors (see Fig. 2 of Supplemental Material [34]). In the framework of weak localization, B_ϕ corresponds to an inelastic scattering length $\ell_\phi = \sqrt{D\tau_\phi} = [\hbar/(4eB_\phi)]^{1/2}$, which is plotted in Fig. 4(a) for different doping x. It is rather constant as a function of gate voltage and estimated to be $\ell_\phi \simeq 45$ nm for $x = 0$, $\ell_\phi \simeq 32$ nm for $x = 0.1$, and $\ell_\phi \simeq 25$ nm for $x = 0.2$. Interestingly, when ℓ_ϕ becomes smaller than the estimated bare superconducting coherence length $\xi \simeq 35$ nm [3], superconductivity is strongly suppressed and T_c goes to zero (for $x = 0.2$). This is consistent with the Finkelstein's scenario where enhanced electron-electron interactions due to disorder destroy superconductivity [28,45].

The spin-orbit field B_{SO} increases monotonically with V_G and ranges between 0.1 to 1 T [Fig. 3(b)] as already observed in undoped samples [4,19,46]. It is remarkable that despite the strong differences discussed above in the transport properties (R, T_c, and B_ϕ, for instance), the B_{SO} term is quasi-identical for the three samples in the whole range of gating. This confirms experimentally that the Dyakonov-Perel mechanism of spin relaxation [29] in the presence of Rashba spin-orbit interaction is dominant in these 2DEG [40]. We found that τ_{SO} is proportional to the inverse scattering time τ_e as shown in Fig. 4(b) for different values of the gate voltage. This is a quantitative and unambiguous signature of the Dyakonov-Perel mechanism. Since $\tau_{SO} \propto \tau_e^{-1}$ and $D \propto \tau_e$, the B_{SO} field [Fig. 3(b)] and the corresponding spin diffusion length $\ell_{SO} = \sqrt{D\tau_{SO}}$ [Fig. 4(a)] are essentially independent of disorder. For the lowest electron density, $\ell_{SO} = [\hbar/(4eB_{SO}]^{1/2} \simeq 40$–$50$ nm is comparable to the inelastic scattering length $\ell_\phi \simeq 25$–40 nm [Fig. 4(a)]. When the 2DEG is strongly electrostatically doped, ℓ_{SO} becomes smaller than ℓ_ϕ ($\ell_{SO} \simeq 15$ nm), indicating that the spin relaxation due to spin-orbit coupling dominates the decoherence processes. Notice that in this analysis, we used a single Drude scattering time τ_e extracted from the sheet resistance. This is justified by the fact that one population of carrier has only a very weak contribution to the total resistance in the gate range where we extract the spin-orbit scattering time (i.e., for $V_G < 120$ V) (see Supplemental Material [34]).

Since B_{SO} and ℓ_{SO} do not vary with disorder (i.e., with τ_e), their evolution with gate voltage must be mainly due to the modification of the coupling constant α upon gating. In the case of a Rashba spin-orbit interaction, α can directly be extracted from B_{SO}: $\alpha = (e\hbar^3 B_{SO})^{1/2}/m$ [29]. Assuming an electron effective mass of $0.7m_e$, which corresponds to d_{xy} subbands mainly populated, we find that α increases linearly with the total carrier density for the three samples [Fig. 4(c)]. Changing the gate voltage modifies the carrier density and self-consistently the shape of the quantum well in which the 2DEG is confined [17]. When electrons are added in the well with a positive gate voltage step, the confinement potential becomes steeper and the interfacial electric field increases. Through the Maxwell-Gauss equation, the carrier density of

the 2DEG can be related to the electric field according to the relation $n \simeq \frac{\epsilon}{e} E_z - n_t$, where ϵ is the dielectric constant of $SrTiO_3$ at the interface and n_t is the carrier density of nonmobile charges trapped in the $SrTiO_3$ substrate. Our results show that for the three samples, the coupling constant α is nearly identical and increases linearly with E_z, in agreement with a Rashba spin-orbit interaction.

In summary, we have investigated the effect of the substitution of Al by Cr on superconductivity and spin-orbit coupling in $LaAl_{1-x}Cr_xO_3/SrTiO_3$ interfaces for three samples corresponding to $x = 0$, 0.1, and 0.2. Cr doping induces disorder in the interfacial quantum well that affects all the carriers and leads to a decrease of the electronic elastic scattering time of the 2DEG, without significant modification of the other parameters. A suppression of superconductivity is observed by increasing the Cr doping consistent with a Finkelstein's reduction of T_c induced by disorder and electron-electron interactions. By analyzing the magnetoconductance of the 2DEG as a function of magnetic field, we showed that the spin diffusion length $\ell_{SO} = \sqrt{D\tau_{SO}}$ is essentially independent of the disorder (i.e., τ_e) and we evidenced a Dyakonov-Perel mechanism of spin relaxation ($\tau_{SO} \propto \tau_e^{-1}$). In addition, we found that the spin-orbit coupling constant α increases linearly with the interfacial electric field E_z which is controlled by the gate voltage, as expected for a Rashba spin-orbit interaction.

Acknowledgments. The authors gratefully thank M. Grilli and S. Caprara for stimulating discussions. This work has been supported by the Région Ile-de-France in the framework of CNano IdF, OXYMORE and Sesame programs, the Delegation Génerale à l'Armement (S.H. Ph.D. grant), CNRS through a PICS program (S2S), and ANR JCJC (Nano-SO2DEG). Part of this work has been supported by the IFCPAR French-Indian program (Contract No. 4704-A). Research in India was funded by the CSIR and DST, Government of India.

[1] A. Ohtomo and H. Y. Hwang, Nature (London) **427**, 423 (2004).
[2] N. Reyren *et al.*, Science **317**, 1196 (2007).
[3] J. Biscaras, N. Bergeal, A. Kushwaha, T. Wolf, A. Rastogi, R. C. Budhani, and J. Lesueur, Nat. Commun. **1**, 89 (2010).
[4] A. D. Caviglia, M. Gabay, S. Gariglio, N. Reyren, C. Cancellieri, and J.-M. Triscone, Phys. Rev. Lett. **104**, 126803 (2010).
[5] M. B. Shalom, C. W. Tai, Y. Lereah, M. Sachs, E. Levy, D. Rakhmilevitch, A. Palevski, and Y. Dagan, Phys. Rev. B **80**, 140403(R) (2009).
[6] L. Li, C. Richter, J. Mannhart, and R. C. Ashoori, Nat. Phys. **7**, 762 (2011).
[7] J. A. Bert, B. Kalisky, C. Bell, M. Kim, Y. Hikita, H. Y. Hwang, and K. A. Moler, Nat. Phys. **7**, 767 (2011).
[8] H. Y. Hwang, Y. Iwasa, M. Kawasaki, B. Keimer, N. Nagaosa, and Y. Tokura, Nat. Mater. **11**, 103 (2012).
[9] H. Takagi and H. Y. Hwang, Science **327**, 1601 (2010).
[10] J. Mannhart and D. G. Schlom, Science **327**, 1607 (2010).
[11] M. Bibes, J. E. Villegas, and A. Barthélémy, Adv. Phys. **60**, 5 (2011).
[12] M. Basletic, J.-L. Maurice, C. Carrétéro, G. Herranz, O. Copie, M. Bibes, E. Jacquet, K. Bouzehouane, S. Fusil, and A. Barthélémy, Nat. Mater. **7**, 621 (2008).
[13] N. Reyren, S. Gariglio, A. Caviglia, D. Jaccard, T. Schneider, and J. M. Triscone, Appl. Phys. Lett. **94**, 112506 (2009).
[14] A. Dubroka, M. Rössle, K. W. Kim, V. K. Malik, L. Schultz, S. Thiel, C. W. Schneider, J. Mannhart, G. Herranz, O. Copie, M. Bibes, A. Barthélémy, and C. Bernhard, Phys. Rev. Lett. **104**, 156807 (2010).
[15] Z. S. Popović, S. Satpathy, and R. M. Martin, Phys. Rev. Lett. **101**, 256801 (2008).
[16] S. Thiel, G. Hammerl, A. Schmehl, C. W. Schneider, and J. Mannhart, Science **313**, 1942 (2006).
[17] J. Biscaras, N. Bergeal, S. Hurand, C. Grossetête, A. Rastogi, R. C. Budhani, D. LeBoeuf, C. Proust, and J. Lesueur, Phys. Rev. Lett. **108**, 247004 (2012).
[18] A. Caviglia, S. Gariglio, N. Reyren, D. Jaccard, T. Schneider, M. Gabay, S. Thiel, G. Hammerl, J. Mannhart, and J.-M. Triscone, Nature (London) **456**, 624 (2008).
[19] S. Hurand *et al.*, Sci. Rep. **5**, 12751 (2015).
[20] S. Hurand *et al.*, Appl. Phys. Lett. **108**, 052602 (2016).
[21] T. Fix, F. Schoofs, J. L. MacManus-Driscoll, and M. G. Blamire, Appl. Phys. Lett. **97**, 072110 (2010).
[22] T. Fix, F. Schoofs, J. L. MacManus-Driscoll, and M. G. Blamire, Phys. Rev. Lett. **103**, 166802 (2009).
[23] M. T. Gray, T. D. Sanders, F. J. Wong, A. J. Grutter, U. S. Alaan, C. He, C. A. Jenkins, E. Arenholz, and Y. Suzuki, Appl. Phys. Lett. **102**, 131601 (2013).
[24] T. D. Sanders, M. T. Gray, F. J. Wong, and Y. Suzuki, Phys. Rev. B **91**, 205112 (2015).
[25] S. Das, A. Rastogi, L. Wu, J.-C. Zheng, Z. Hossain, Y. Zhu, and R. C. Budhani, Phys. Rev. B **90**, 081107(R) (2014).
[26] S. A. Chambers, L. Qiao, T. C. Droubay, T. C. Kaspar, B. W. Arey, and P. V. Sushko, Phys. Rev. Lett. **107**, 206802 (2011).
[27] R. Colby, L. Qiao, K. H. L. Zhang, V. Shutthanandan, J. Ciston, B. Kabius, and S. A. Chambers, Phys. Rev. B **88**, 155325 (2013).
[28] A. M. Finkelstein, Physica B: Condens. Matter **197**, 636 (1994).
[29] M. I. Dyakonov and V. I. Perel, Sov. Phys. Solid State **13**, 3023 (1972).
[30] P. Kumar, A. Dogra, P. P. S. Bhadauria, A. Gupta, K. K. Maurya, and R. C. Budhani, J. Phys.: Condens. Matter **27**, 125007 (2015).
[31] J. Biscaras, S. Hurand, C. Feuillet-Palma, A. Rastogi, R. C. Budhani, N. Reyren, E. Lesne, J. Lesueur, and N. Bergeal, Sci. Rep. **4**, 6788 (2014).
[32] J. S. Kim, S. S. A. Seo, M. F. Chisholm, R. K. Kremer, H.-U. Habermeier, B. Keimer, and H. N. Lee, Phys. Rev. B **82**, 201407 (2010).
[33] R. Ohtsuka, M. Matvejeff, K. Nishio, R. Takahashi, and M. Lippmaa, Appl. Phys. Lett. **96**, 192111 (2010).
[34] See Supplemental Material at http://link.aps.org/supplemental/10.1103/PhysRevB.96.024509 for more experimental results.
[35] N. Nakagawa, H. Y. Hwang, and D. A. Muller, Nat. Mater. **5**, 204 (2006).
[36] S. Caprara, J. Biscaras, N. Bergeal, D. Bucheli, S. Hurand, C. Feuillet-Palma, A. Rastogi, R. C. Budhani, J. Lesueur, and M. Grilli, Phys. Rev. B **88**, 020504 (2013).

[37] J. Biscaras, N. Bergeal, S. Hurand, C. Feuillet-Palma, A. Rastogi, R. C. Budhani, M. Grilli, S. Caprara, and J. Lesueur, Nat. Mater. **12**, 542 (2013).
[38] N. Scopigno, D. Bucheli, S. Caprara, J. Biscaras, N. Bergeal, J. Lesueur, and M. Grilli, Phys. Rev. Lett. **116**, 026804 (2016).
[39] C. Richter, H. Boschker, W. Dietsche, E. Fillis-Tsirakis, R. Jany, F. Loder, L. F. Kourkoutis, D. A. Muller, J. R. Kirtley, C. W. Schneider and J. Mannhart, Nature (London) **502**, 528 (2013).
[40] Y. A. Bychkov and E. I. Rashba, J. Phys. C **17**, 6039 (1984).
[41] R. Winkler, *Spin-Orbit Coupling Effects in Two-Dimensional Electron and Hole Systems* (Springer, Berlin, 2003).
[42] S. Maekawa and H. Fukuyama, J. Phys. Soc. Jpn. **50**, 2516 (1981).
[43] S. Hikami, A. I. Larkin, and Y. Nagaoka, Y. Prog. Theor. Phys. **63**, 707 (1980).
[44] D. K. C. Macdonald and K. Sarginson, Rep. Prog. Phys. **15**, 249 (1952).
[45] P. A. Lee and T. V. RamakrishnanRev. Mod. Phys. **57**, 287 (1985).
[46] G. Herranz, G. Singh, N. Bergeal, A. Jouan, J. Lesueur, J. Gázquez, M. Varela, M. Scigaj, N. Dix, F. Sánchez, and J. Fontcuberta, Nat. Commun. **6**, 6028 (2015).